

Study of Plastic Deformation in Hexagonal Metals by Interrupted In-Situ EBSD Measurement

Lei Bao, Jean-Sébastien Lecomte, Christophe Schuman, Marie-Jeanne Philippe, Xiang Zhao, Claude Esling

▶ **To cite this version:**

Lei Bao, Jean-Sébastien Lecomte, Christophe Schuman, Marie-Jeanne Philippe, Xiang Zhao, et al.. Study of Plastic Deformation in Hexagonal Metals by Interrupted In-Situ EBSD Measurement. Advanced Engineering Materials, 2010, 12 (10), pp.1053 - 1059. 10.1002/adem.201000074 . hal-03864520

HAL Id: hal-03864520
https://cnrs.hal.science/hal-03864520

Submitted on 26 Dec 2022

HAL is a multi-disciplinary open access archive for the deposit and dissemination of scientific research documents, whether they are published or not. The documents may come from teaching and research institutions in France or abroad, or from public or private research centers.

L'archive ouverte pluridisciplinaire **HAL**, est destinée au dépôt et à la diffusion de documents scientifiques de niveau recherche, publiés ou non, émanant des établissements d'enseignement et de recherche français ou étrangers, des laboratoires publics ou privés.

Study of plastic deformation in hexagonal metals by interrupted in-situ EBSD measurement

Lei Bao [a,b], Jean-Sébastien Lecomte [a], Christophe Schuman [a], Marie-Jeanne Philippe [a], Xiang Zhao [b], Claude Esling [a]*

[a] *LETAM, CNRS FRE 3143 (former UMR 7078) University of Metz, 57045 Metz, France*

[b] *Key Lab for Anisotropy and Texture of Materials (Ministry of Education), Northeastern University, Shenyang, 110004 China*

[*]claude.esling@univ-metz.fr

Abstract. The present work was undertaken to provide information, lacking in the literature, on the lattice rotation and the role of twinning during cold rolling of commercial purity titanium (T40). The proposed method consists of determining the individual rotation of the grains induced by low to intermediate deformation (up to 30% in thickness reduction) and following the rotation field using electron backscattered diffraction (EBSD) measurements in a high resolution FEG SEM at different steps of deformation (10 and 20 %). We have especially studied the formation, the evolution and the role of mechanical twins.

According to the former research, during deformation at room temperature, three different types of twin systems were activated: $\{10\bar{1}2\}$ tensile twinning, $\{11\bar{2}2\}$ compression twinning and – to a small extent - $\{11\bar{2}1\}$ tensile twinning, depending on the grain orientation. Secondary twins (often $\{10\bar{1}2\}$ within $\{11\bar{2}2\}$ twins) were activated in the grains oriented favourably for this secondary twinning. This resulted in a heterogeneous microstructure in which grains were refined in some areas. It also induced re-orientation of the c-axes to stable orientations. No twins of higher order than the second order twins could be found.

The rotation flow field was measured by following the rotation of 800 grains. It was possible to determine the individual grains rotations as well as the average flow field. For grains having twinned parts, the lattice rotation of the matrix is similar to that of the grains having a similar crystallographic orientation but without any twin. Twins form in grains having specific orientations with respect to the macroscopic stress field; they can grow in the grain with increasing strain and may consume almost the whole matrix.

Keywords: *Titanium; Rolling; Rotation flow field; Gliding; Twinning; Texture.*

Introduction

The titanium textures observed at room temperature in the α hexagonal close-packed (HCP) structure are inherited to some extent from their prior texture in the β body centred cubic (BCC) structure [1]. However most of the research effort concentrated on the strong deformation textures that Titanium [2-4], like other HCP metals, develops during the rolling at room temperature, that lead to a pronounced plastic anisotropy of the polycrystalline materials [5]. The mechanical response of HCP metals is strongly dependent on the combination of active deformation modes: slip and twinning. The specific deformation mechanisms depend on the c/a ratio, the available deformation modes, the critical resolved shear stress (CRSS) for slip and the twin activation stress, as well as the imposed deformation relative to the crystallographic texture. For pure

titanium, $\{10\bar{1}0\}<11\bar{2}0>$ slip is the primary deformation mode. This slip mode alone, however, cannot accommodate the imposed strain in the grains of a polycrystalline aggregate, because it cannot provide 5 independent slip systems [4, 6-9]. Additional deformation mechanisms such as pyramidal planes with <c+a> Burger's vector or twinning usually have to be activated. The observed ductility has been attributed essentially to the occurrence of twinning on the $\{11\bar{2}1\}$ and $\{11\bar{2}2\}$ planes.
Chun et al. [10] studied the effect of deformation twinning on microstructures during cold rolling of commercially pure (CP) titanium. The primary twinning systems activated were $\{11\bar{2}2\}<11\bar{2}3>$ compressive twins and $\{10\bar{1}2\}<10\bar{1}1>$ tension twins. Secondary twins, mainly of the tensile type, were also activated.
In order to describe the texture evolution, different models of polycrystalline plasticity are used. Polycrystal plasticity models are routinely employed to predict deformation textures. Wu et al. [11] employed a new Taylor type of crystal plasticity model to predict the texture evolution and anisotropic stress-strain curves in α-titanium. The main features of this model include: (i) incorporation of slip inside twins as a significant contributor to accommodating the overall imposed plastic deformation; and (ii) extension of slip and twin hardening laws to treat separately the hardening behaviour of the different slip families (prismatic <a>, basal <a> and pyramidal <c+a>) using hardening parameters that are all coupled to the extent of deformation twinning in the sample. Proust et al. [12] developed a model which takes into account the texture evolution associated with twin reorientation and the effect of the twin barriers on dislocation propagation. The role of the twins as barriers to dislocations was explicitly incorporated into the hardening description via geometrically necessary dislocations (GNDs) and a directional Hall-Petch mechanism. However, with these complex models, the lack of direct experimental information on slip and twinning systems imposes difficulties for the related modelling practices.
The present work was undertaken to provide information, lacking in the literature, on the lattice rotation and the role of twinning during cold rolling of commercial purity titanium (T40). The method proposed consists of determining the individual rotation of the grains induced by low to intermediate deformation (up to 30% in thickness reduction) and to following the rotation field using electron backscattered diffraction (EBSD) measurements in a high resolution FEG SEM at different steps of deformation (10 and 20 %). We have especially studied the formation, the evolution and the role of mechanical twins. Additional work on identification of slip systems by two different approaches (deformation experiments on single crystals as well as numerical *ab initio* and molecular dynamics calculations) are being developed in parallel.

Experimental

The as-received material was hot-rolled and then annealed commercial pure titanium sheet of 1.5 mm thickness with the composition is given in table 1.

Table 1 Chemical composition of commercially pure titanium T40

Element	H	C	N	O	Fe	Ti
Composition (ppm (wt.))	3	52	41	1062	237	Balance

In order to obtain a microstructure with a mean grain size of 30 µm, a grain growth anneal was performed at 750°C for 2 hours. After annealing, the samples were mechanically ground and then electrolytically-polished in a solution of 20 ml perchloric acid in 80 ml methanol at 17V (30 seconds) and a temperature of 5°C before the cold rolling. Then, the samples were cold rolled in two passes, first to 10 % and then to 20% reduction. The cold rolling was performed in the transverse direction of the former hot rolling in order to induce significant reorientations of the C- axes of the grains. To follow the rotation of the individual grains

during the deformation, a 500×300 μm2 area was carefully polished and marked out with four micro-indentations. The orientation of all the grains in this polished area (about 800 grains) was measured by SEM/EBSD before and after each deformation step. The rolling layout is illustrated in Fig. 1. Both sheets of the sandwich were firmly stuck together to avoid any surface sliding during the rolling in order to maintain a good surface quality. EBSD measurements were performed with a JEOL-6500F SEM with a step size of about 0.77 μm. The evolution of grain orientation during deformation will be presented later both by pole figures and lattice rotation fields.

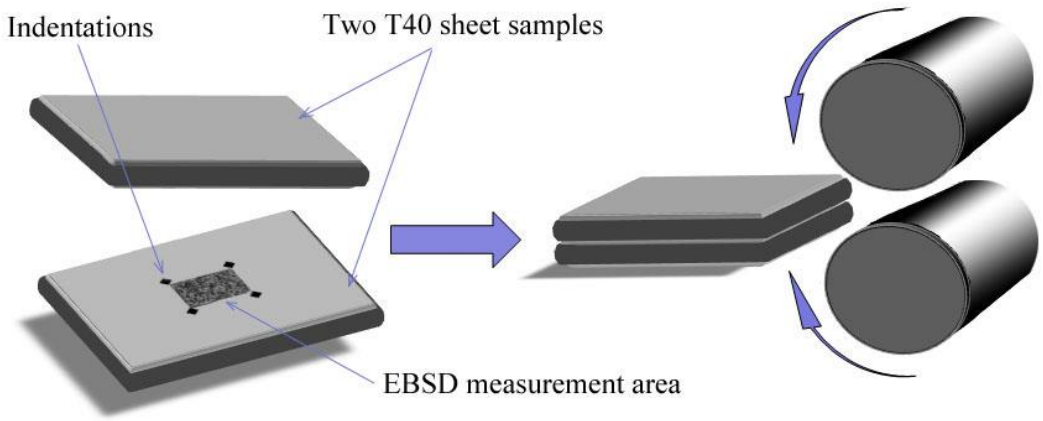
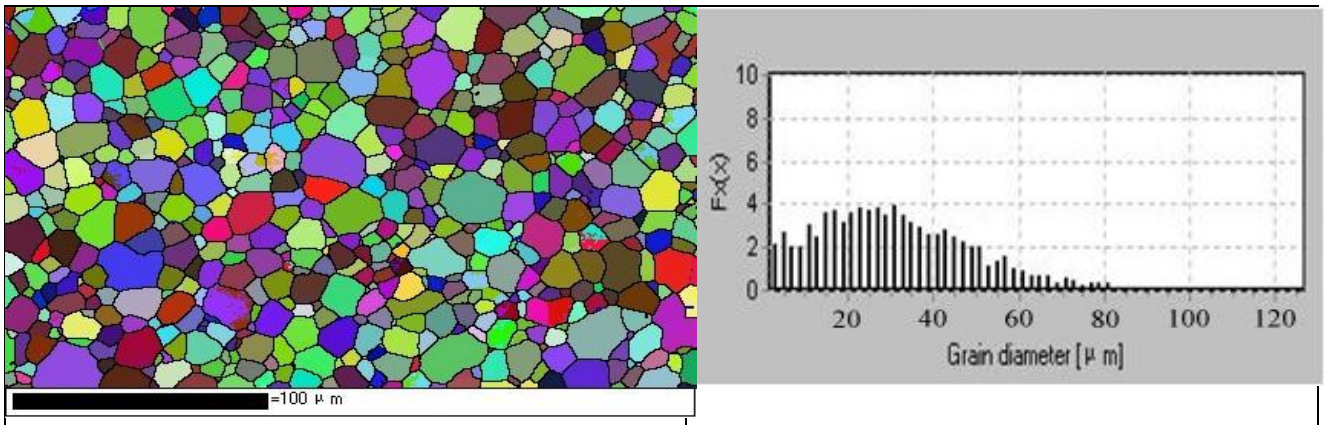


Fig. 1 Successive cold-rolling was performed on sandwich samples. The inner surface was initially polished and the orientation of the grains was measured by EBSD before and after each rolling step.

Results

1. Initial microstructure and texture

The orientation map of the grain growth annealed sample shown in Fig. 2 reveals a completely recrystallized microstructure. No twins were observed as metals with HCP structure do not undergo recrystallization twinning. The{0002}-pole figure (PF) in Fig. 3 shows two strong maxima at ±35° tilted from ND towards TD, the setting of the coordinate systems and the definition of the Euler angles being in accordance to Bunge's convention, see e.g. [13]. The $\{10\bar{1}0\}$ PF displays the maximum pole densities parallel to RD.



(a) (b)

Fig. 2 (a) Orientation micrograph of the microstructure prior to deformation for the CP-titanium and (b) its grain size distribution

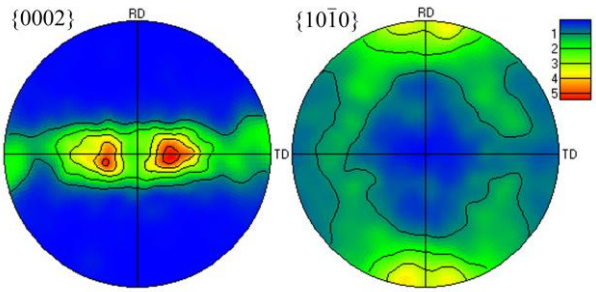
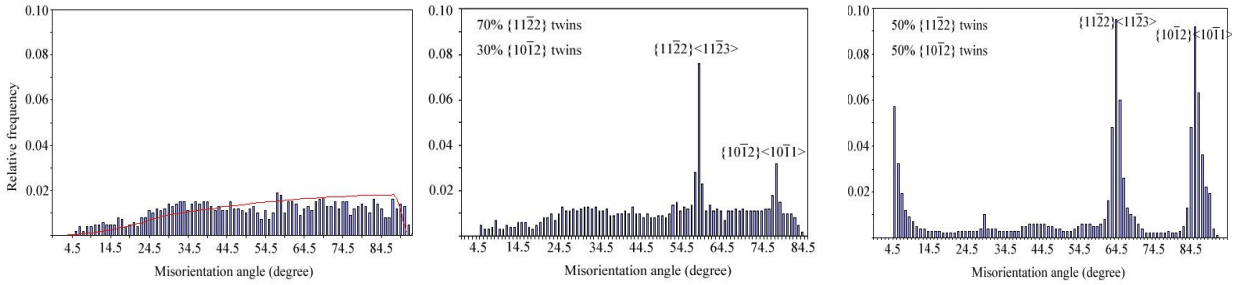


Fig. 3 Pole figures of the CP-Ti sheet after the grain growth annealing. The texture is dominated by the orientation E ($\phi 1 = 0°$, $\Phi=30°$, $\phi 2=30°$) characterized by $\{0002\}<11\bar{2}0>$ tilted 30° from ND towards TD

2. Evolution of the microstructure during cold rolling: effect of twinning

The lattice rotation was studied after each deformation pass. The orientation of each individual grain was carefully determined, so that the lattice rotation of each grain could be brought in relation to the orientation to its own orientation as well as to that of its neighbouring grains. It was found that $\{11\bar{2}2\}<11\bar{2}\bar{3}>$ compression twins (the misorientation between the twin and its matrix corresponds to 65 °

rotation about their common $<10\bar{1}0>$ axis) and $\{10\bar{1}2\}<10\bar{1}\bar{1}>$ tension twins (85° about $<11\bar{2}0>$) were most frequently observed. The respective amount of these two twinning modes was further presented by means of the misorientation-angle distributions in Fig. 4. It is seen that at 10% deformation (Fig. 4 (b)), 65° misorientation occurs most frequently, suggesting that $\{11\bar{2}2\}$ twinning was predominant at this deformation stage. This result is reasonable considering that the initial orientation favors the occurrence of this compression twin. Whereas when deformation continues to 20%, $(10\bar{1}2)$ tension twinning was remarkably increased (Fig. 4 (c)). Although Fig.4 (c) shows a small peak around the misorientation of 30°, close to the misorientation angle of the $\{11\bar{2}1\}$ tension twin, the corresponding misorientation axis does not correspond to the $\{11\bar{2}1\}$ tension twin, which can thus be excluded in the sample studied.



(a) (b) (c)

Fig. 4 Misorientation-angle distributions of samples deformed to (a) 0%, (b) 10% and (c) 20% reduction.

3. Lattice rotation fields and texture development

The orientation analysis could be studied from the microscopic viewpoint of the crystal reorientation step by step, in terms of the lattice rotation flow field. A small arrow is plotted between the initial grain orientation and the final grain orientation. This field of small arrows offers a graphical representation of the flow field. The orientation flow field can be defined and plotted in the Euler space, and represents an efficient tool to describe the texture evolution through modeling, e.g. Clement and Coulomb (1979) [14], Bunge and Esling (1984) [15]. In the present case of hexagonal material, due to the particular importance of the c-axes, we choose to plot the small arrows linking the initial orientation and the final orientation in the two dimensional pole figures of the c-axes. For the further discussion, it was of interest to plot separately the rotation flow field of the grains having no twinned part on the one hand (Fig.5 (a)) and the rotation flow field of the matrix part of the grains presenting twinned parts inside the grains (Fig. 5 (b)). Both orientation flow fields are similar, but for a smaller amplitude of the rotation of the matrix of twinned grains, as compared to the grains without twins.

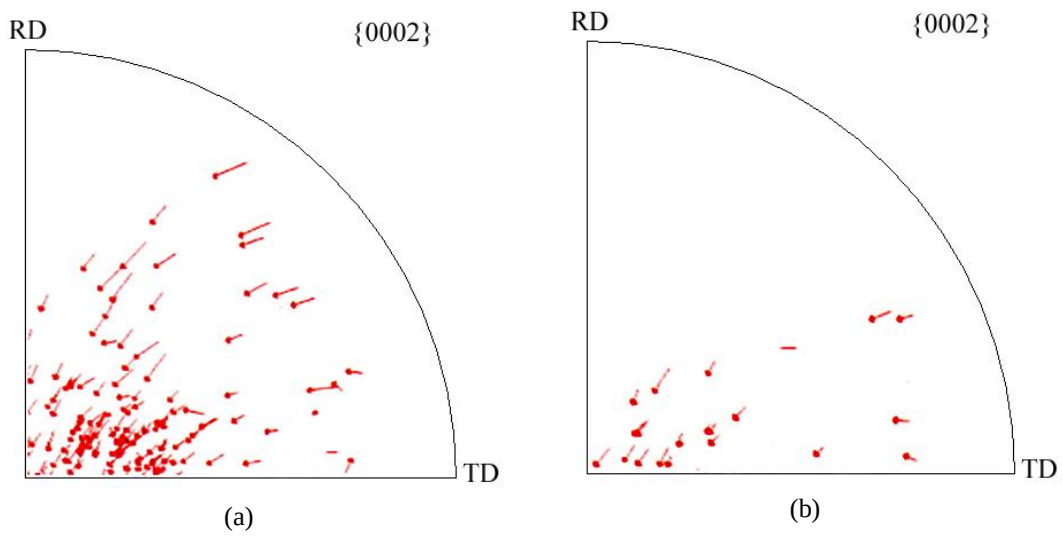
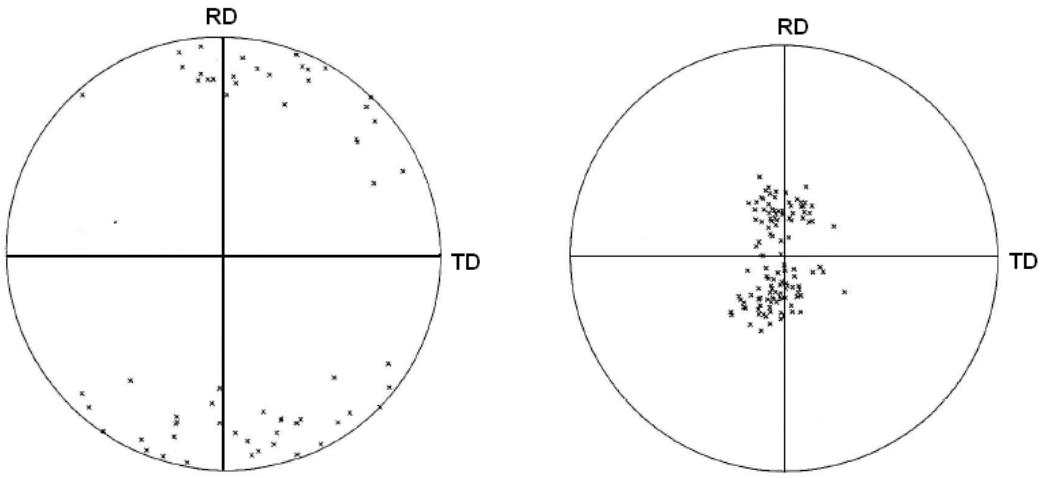


Fig. 5 (a) Lattice rotation field in grains showing no twins. (b) Lattice rotation field in untwinned part or matrix of grains showing twins.

The orientation analysis could be also studied from the macroscopic viewpoint of development of crystallographic texture, and presented in the classical representation of pole figures. Orientation analysis indicates that at 10% reduction, the c-axis of the grains with $\{10\bar{1}2\}$ twins (tension along c-axis) is oriented close to the rolling direction, as shown in Fig. 6 (a); whereas that of the grains with $\{11\bar{2}2\}$ twins (compression along c-axis) is oriented close to the sample normal direction, as shown in Fig. 6 (b). These results are coherent with the theory (Fig. 7). The c-axis of the $\{10\bar{1}2\}$ and $\{11\bar{2}1\}$ twinned part in each grain is systematically oriented close to a stable orientation belonging to the rolling texture component, however, the $\{11\bar{2}2\}$ twinning leads the c-axis of the twinned part oriented close to the rolling direction i.e. to an unstable orientation. As shown in Fig. 8, the $\{10\bar{1}2\}$ tension twinning results in a 84.78° reorientation of the c-axis as schematized by the blue arrow, whereas the $\{11\bar{2}2\}$ compression twinning results in a 64.62° reorientation of the c-axis as schematized by the red arrow. The green area delimits the stable orientation of the c axes belonging to the rolling texture (<c> axes tilted about 30°from ND (Normal Direction) in the ND-TD plane (Transverse Direction). Form the figure, it is clear that the $\{10\bar{1}2\}$ twinning transfers the orientation of the matrix to the stable orientation of the rolling texture whereas $\{11\bar{2}2\}$ twinning acts reversely.



(a) (b)

Fig. 6 (a) {0002} -Pole figure of grains having $\{10\bar{1}2\}$ twin and (b) {0002} Pole Figure of grains having $\{11\bar{2}2\}$ - Twin (10% deformation).

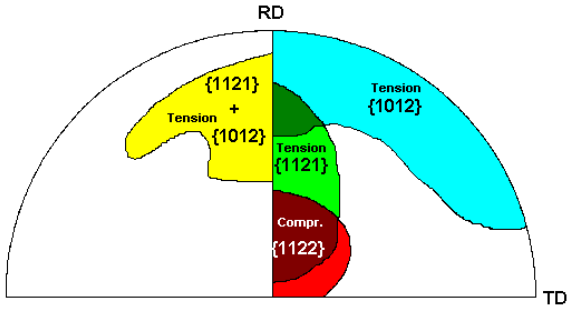


Fig. 7 (0002) Pole Figure showing schematically the orientation domains of the c-axes of the grains in which the indicated twinning is expected to be activated (theoretical)

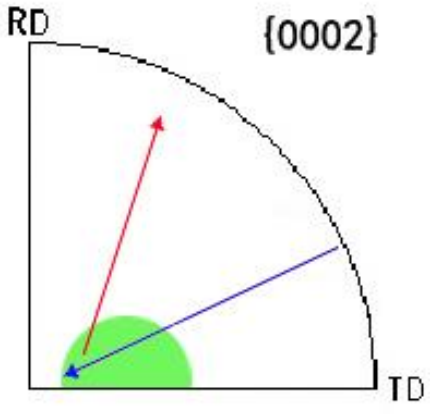
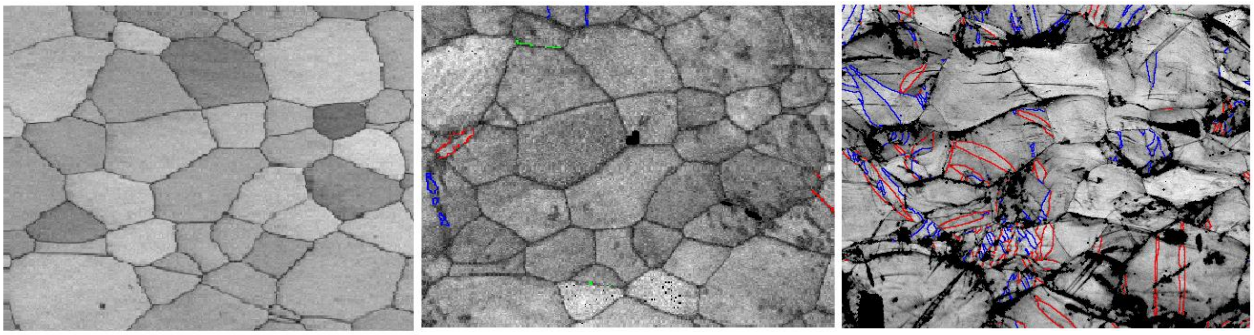


Fig. 8 Reorientation of c axes resulting from the $\{10\bar{1}2\}$ tension twinning (blue arrow) and from $\{11\bar{2}2\}$ compression twinning (red arrow).

4. Secondary twinning

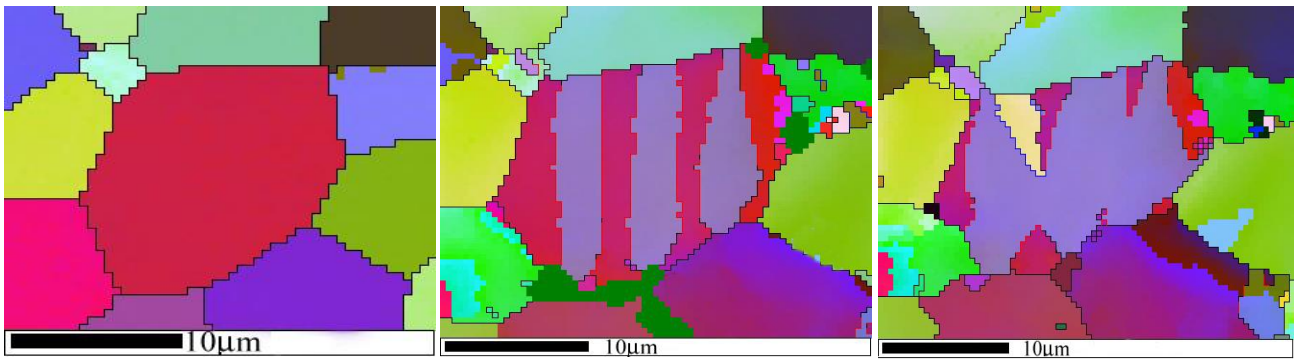
Due to the technique used in the present work, we can follow the evolution of the twins in each grain. Fig. 9 shows one selected sample area before and after each deformation pass. In the figure, the blue lines represent the $\{10\bar{1}2\}$ twin boundaries and the red lines the $\{11\bar{2}2\}$ twin boundaries. Interestingly it is found that tension twins and compression twins can coexist in one and the same grain (Fig. 9). This might be not obvious to understand since both twin modes require utterly different grain orientation in order to get activated (cf. Fig. 7) and two contrasting loading modes; i.e. c-axis compression and c-axis tension. But this is mainly observed at higher deformation (20% rolling) and in the form of double twins, with secondary tensile twins appearing in primary compression twin.



(a) (b) (c)

Fig. 9 Orientation micrograph of one selected area (a) before rolling, after (b) 10% and (c) 20% rolling. Blue lines: $\{10\bar{1}2\}$ twin boundaries; red lines: $\{11\bar{2}2\}$ twin boundaries

Fig. 10 shows a grain with its c-axis oriented close to the sample normal direction (ND). The $\{11\bar{2}2\}$ compression twins appear when the deformation reaches 10% (Fig. 10(b)). However, when deformation reaches 20%, the $\{11\bar{2}2\}$ twin spreads to merge across almost the entire grain and then the $\{10\bar{1}2\}$ tension twin is activated in the interior of the $\{11\bar{2}2\}$ twin. This occurrence of second order twins can be observed in all such oriented grains. Without the initial orientation information of the grain, we could not easily have distinguished the initial matrix from the twins. In fact after 10% deformation, the initial matrix shrinks considerably; with residues remaining just between the compression twins such that the large twinned area becomes the "new matrix" for the further tension twins.



(a) (b) (c)

Fig. 10 (a) Initial grain with c axis oriented close to the normal direction (red); (b) 10% deformation: $\{11\bar{2}2\}$ compression twins outlined by red lines; (c) 20% deformation: a part of $\{11\bar{2}2\}$ twins undergoes secondary $\{10\bar{1}2\}$ tension twinning, as outlined by blue twinning boundaries delimiting the tension twin (in yellow color).

This appearance of the $\{10\bar{1}2\}$ tension twin inside the $\{11\bar{2}2\}$ compression twin is the so-called secondary twinning. In fact, as we have indicated, the formation of $\{11\bar{2}2\}$ twinning brings the c-axis of the twinned part far out of the stable orientation range. The twinned part is favorably oriented to initiate a tension twin. Then the $\{10\bar{1}2\}$ tension twin forms, bringing the c-axis of the newly twinned part to a stable orientation. The trajectory of the c-axes orientation evolution during these twinning processes is indicated in the {0002} pole figure, Fig. 11.

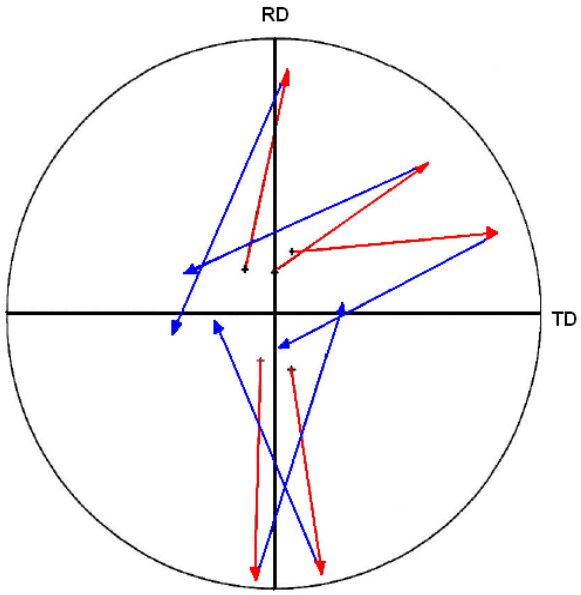
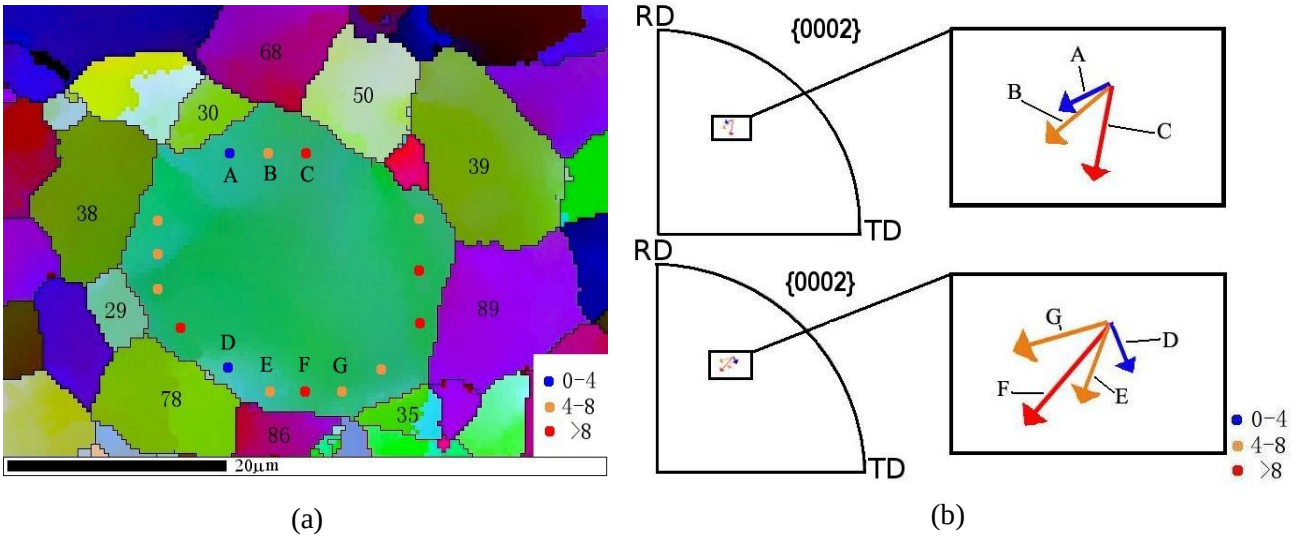


Fig. 11 Trajectory of the reorientation by $\{10\bar{1}2\}$ secondary twinning in $\{11\bar{2}2\}$ primary twins. Red: reorientation by $\{11\bar{2}2\}$ compression twins; blue: reorientation by $\{10\bar{1}2\}$ tension twins.

5. Effect of the orientation of the neighbouring grains: heterogeneous deformation

In large grains, different domains in the one and the same grain may undergo different lattice rotations. Fig. 12 presents a large grain (green color) in which several parts have experienced different lattice rotations. The numbers inside the small neighboring grains give the misorientations of the c-axes with respect to the c-axis corresponding to the mean orientation of the large green grain. We can study here the respective rotations of the domains inside the large green grain, notably in the neighbourhood of the grain boundary, and thus estimate the influence of the neighbouring grains. In any case the rotation of the grain interior is smaller than that of the part close to the grain boundary, especially when the neighbouring grains are highly misoriented with respect to the investigated domain.



(a) (b)

Fig. 12 Effect of the neighboring grains on the lattice rotation. (a) Misorientation of the c-axes of neighboring grains (numbers inside the neighboring grains) with respect to the large grain they surround and reorientation of the c-axis in the regions A, B…in the neighborhood of the grain boundary (color code in the inset). (b) Illustration of the reorientation of the c axes in the various boundary regions A, B…of the large green grain.

Discussion

Comparison of the rotation of the matrix part of the grains containing twins with the rotation of the untwinned grains indicates that the lattice rotation in the two cases are similar, even if the amplitude of the rotation in the non-twinned part of the twinned grains is relatively smaller.

This tends to show that the main effect of twinning is to create a newly oriented zone (a new grain) and does not induce additional deformation mechanisms in the remaining matrix part of the grain. In other words, the deformation mechanisms in the matrix part of the twinned grains remain the same as those in the untwinned grains. The reorientation induced by $\{11\bar{2}1\}$ and $\{10\bar{1}2\}$ twinning tends to orientate the c-axes close to stable orientations. Thus, there is no tendency for secondary twinning to occur within such twins.

The secondary twinning only takes place in the $\{11\bar{2}2\}$ compression twins whose c-axes are orientated far away from the stable texture orientation. In such a case, the new and major twins appearing inside the $\{11\bar{2}2\}$ twins are $\{10\bar{1}2\}$ tension twins. This explains why when deformation is increased from 10% to 20% the amount of $\{10\bar{1}2\}$ tension twin drastically increases. The c-axis of this secondary twin orientates towards to the stable orientation. Most probably the primary compression twins result from the shear induced in the twinning system submitted to the highest resolved shear stress imposed by the rolling stress. Then the secondary tension twin can be activated for two reasons. First in the compression twin the crystal lattice is reoriented favorably for subsequent tensile twin. Second, the shear imposed by the first twinnig creates local a stress state in reaction to the primary shear (back stress), which is not anymore the resolved

stress as applied by the roller. We could hardly observe the presence of any third-order twin, even after much higher deformation. This can be easily understood by the relation between the geometrical and energetical characteristics of twinning (and by the mean free path necessary for the formation of a twin). In fact, in titanium alloys it is difficult to induce twinning once the grain size in the matrix drops below the range of about 10 µm.
The great benefit of the present method is that we can follow the deformation process step by step. For example, in the grains having their initial c-axis close to ND for which secondary twinning occurs inside the primary twins, we can clearly discriminate the initial matrix from the primary twins thanks to the in-situ orientation information. In this case the primarily twinned area is much larger than the remaining matrix and thus represents the "new matrix" for the subsequent secondary twinning.
The effect of the neighboring grains slightly modifies the orientation in the vicinity of the grain boundary, and leads to a larger spread in orientation when the neighboring grain is strongly misoriented with respect to the considered grain. The detailed experimental study of the complex twinning conditions in hexagonal materials may be helpful to the implementation of mechanical twinning in models and codes of polycrystalline plasticity. A thorough study of the implementation of mechanical twinning in a Grain Interaction Model and the application to magnesium alloys [16]. can be read with interest in this special volume AEM volume.

Conclusion

Twinning occurs in grains that have particular orientations. Generally, the reorientation induced by twinning aligns the c-axis of the twinned part to the stable rolling texture orientations, so that no further secondary twinning can be induced. Secondary twinning occurs only when the primary twinning orientates the c-axis of the primary twins far away from the stable orientations (this is generally the case for the $\{11\bar{2}2\}$ twinning). The formation of the $\{10\bar{1}2\}$ secondary twin inside the $\{11\bar{2}2\}$ primary twin results in a reorientation of the c-axis of the secondary twin to a stable orientation. The primary compression twins results from the shear induced in the twinning system submitted to the highest resolved shear stress imposed by the rolling stress, whereas the secondary tension twin can be activated because of the reorientation of the lattice in the compression twin and the local stress conditions in reaction to the primary twinning shear (back-stress). Only a little amount of second order twinning could be observed and twinning of higher than second order was never found.
The rotation of the matrix-part of the grains having twins is similar to that of the non-twinned grains with similar orientation. The twinned part of a grain can be considered as a new grain. When twins grow within the grain, they can consume almost the whole matrix. Special attentions should be paid when determining the twinned volume fraction. Thanks to the EBSD measurement, a strong increase of the twinned volume could be demonstrated. This contradicts the conventional judgement that the twinned part is always the smaller part in a twinned grain, as concluded by optical microscopy. Only step by step EBSD orientation mapping allows an unambiguous determination of the twinned volume fraction. The confirmation that the order of twinning never exceeds the second order is very useful for the modelling of plasticity in polycrystalline metals, such that the order allowed for twins should be restricted to only the first and second order (also called double twins).

Acknowledgements

This work is supported by the FRAE project OPTIMIST and the French CNRS (PICS No. 4164). The authors would like to express their thanks to Dr. Yudong Zhang for contributing to the EBSD measurements and

improving the English wording of the paper. The first author, Lei Bao is grateful for a PhD grant from China Scholarship Council. The authors also thank an anonymous reviewer for constructive comments and the acting co-editor, Dr. Talal Al-Samman for the efficient handling of the manuscript.

References

N. Gey, M. Humbert, M. J. Philippe, Y, Combres, Mater. *Sci. Eng. A.* **1997**, *230*, 68.
H. P. Lee, C. Esling, H. J. Bunge, *Textures and Microstructures*. **1988**, *7*, 317.
M. J. Philippe, C. Esling, B. Hocheid, *Textures and Microstructures*. **1988**, *7*, 265.
M. J. Philippe, M. Serghat, P. V. Houtte, C. Esling, *Acta Metall*. **1995**, *43*, 1619.
J. J. Fundenberger, M. J. Philippe, F. Wagner, C. Esling, *Acta Mater.* **1997,** *45*, 4041.
A. Akhtar, *Metall. Mater. Trans. A.* **1975**, *6*, 1105.
P. G. Partridge, *Metall Rev*. **1967,** *12*, 169.
G. W. Groves, A. Kelly, *Phil Mag*. **1963,** *8*, 877.
D. R. Thornburg, H. R. Piehler, *Titanium Sci. Technol*, *Plenum Press.* **1973**, *2*, 1187.
Y. B. Chun, S. H. Yu, S. L. Semiatin, S. K. Hwang, Mater. *Sci. Eng. A.* **2005**, *398*, 209.
X. Wu, S. Kalidindi, C. Necker, A. Salem, *Acta Mater*. **2007**, *55*, 423.
G. Proust, C. Tomé, G. Kaschner, *Acta Mater*. **2007**, *55*, 2137.
H. J. Bunge, C. Esling, J. Muller, J. Appl. Crystallogr., **1980**, 13, 544
A. Clement, P. Coulomb, *Scripta Metall.* **1979**, *13*, 899.
H. J. Bunge, C. Esling, *Scripta Metall.* **1984**, *18*, 191.
S. Mu, T. Al-Samman, Volker Mohles, G. Gottstein, *This AEM volume.*